Synthesis and biomedical applications of functionalized fluorescent and magnetic dual reporter nanoparticles as obtained in the miniemulsion process



2006 J. Phys.: Condens. Matter 18 S2581

(http://iopscience.iop.org/0953-8984/18/38/S04)

INSTITUTE OF PHYSICS PUBLISHING JOURNAL OF PHYSICS: CONDENSED MATTER

J. Phys.: Condens. Matter **18** (2006) S2581–S2594 doi:10.1088/0953-8984/18/38/S04

# Synthesis and biomedical applications of functionalized fluorescent and magnetic dual reporter nanoparticles as obtained in the miniemulsion process

**Verena Holzapfel[1], Myriam Lorenz[1,2], Clemens Kilian Weiss[1], Hubert Schrezenmeier[2], Katharina Landfester[1] and Volker Mailänder[2]**

[1] University of Ulm, Department of Organic Chemistry III—Macromolecular Chemistry and Organic Materials, Albert-Einstein-Allee 11, 89081 Ulm, Germany
[2] University of Ulm, Department of Transfusion Medicine, Institute for Clinical Transfusion Medicine and Immunogenetics, Helmholtzstraße 10, 89081 Ulm, Germany

E-mail: katharina.landfester@uni-ulm.de and v.mailaender@blutspende.de

Received 2 May 2006, in final form 27 July 2006
Published 8 September 2006
Online at stacks.iop.org/JPhysCM/18/S2581

**Abstract**

As superparamagnetic nanoparticles capture new applications and markets, the flexibility and modifications of these nanoparticles are increasingly important aspects. Therefore a series of magnetic polystyrene particles encapsulating magnetite nanoparticles (10–12 nm) in a hydrophobic poly(styrene-*co*-acrylic acid) shell was synthesized by a three-step miniemulsion process. A high amount of iron oxide was incorporated by this process (typically 30–40% (w/w)). As a second reporter, a fluorescent dye was also integrated in order to obtain 'dual reporter particles'. Finally, polymerization of the monomer styrene yielded nanoparticles in the range 45–70 nm. By copolymerization of styrene with the hydrophilic acrylic acid, the amount of carboxyl groups on the surface was varied. The characterization of the latexes included dynamic light scattering, transmission electron microscopy, surface charge and magnetic measurements. For biomedical evaluation, the nanoparticles were incubated with different cell types. The introduction of carboxyl groups on the particle surfaces enabled the uptake of nanoparticles as demonstrated by the detection of the fluorescent signal by fluorescent activated cell sorter (FACS) and laser scanning microscopy. The quantity of iron in the cells that is required for most biomedical applications (like detection by magnetic resonance imaging) has to be significantly higher, as can be achieved by the uptake of magnetite encapsulated nanoparticles functionalized only with carboxyl groups. A further increase of uptake can be accomplished by transfection agents like poly-L-lysine or other positively charged polymers. This functionality was also engrafted into the surface of the nanoparticles by covalently coupling lysine to the carboxyl groups. The amount of iron that can be transfected was even higher than with the nanoparticles with a transfection agent added and this only physically

adsorbed. Furthermore, the subcellular localization of these nanoparticles was demonstrated to be clustered in endosomal compartments.

(Some figures in this article are in colour only in the electronic version)

## 1. Introduction

The characteristics of magnetic nanoparticles make them interesting for biomedical applications [1]. Magnetic particle aggregates stabilized by hydrophilic (water-soluble) polymers are small enough to enter cells or pass borders like the blood–brain barrier [2]. Their surface can be functionalized for selective interaction and their magnetic properties make them controllable by an external magnetic field. The controllability includes magnetic separations as well as far more complicated methods such as magnetic resonance imaging [3], guided drug-delivery, or hyperthermia [4]. The superparamagnetism of the particles ensures that no further aggregation or even coagulation of the particles occurs during and after patient treatment with a magnetic field. Aggregation and coagulation to large particle clusters could have fatal effects, especially in small blood vessels.

Among the magnetic materials with suitable properties, magnetite is the only one that has up to now been allowed for use in humans. It is the only material which is known to be biocompatible, without relevant toxicity in the applied dosing range. Once injected into the blood stream, the particles will stay in the body until they are washed out through the liver and kidney or metabolized by phagocytic cells [5]. The systems used right now are magnetite nanoparticles with a size of about 10 nm, stabilized by hydrophilic polymeric shells like dextrane or carbodextrane. By functionalizing the shell, it is possible to attach for example drugs by ionic links that can be set free at a desired site after being directed there by an external magnetic field [6]. It has been shown that magnetite nanoparticles produce enough heat in an alternating magnetic field to be applied in hyperthermia treatment [7].

To improve the properties of the magnetite nanoparticles in regard to iron leakage and aggregation or coagulation, the magnetic nanoparticles can be efficiently encapsulated in a hydrophobic polymer shell [8, 9]. This encapsulation ensures that the shell is not washed off in hydrophilic media, which would result in sedimentation and aggregation of the magnetic core particles. At the same time, high magnetite contents and uniform distribution of magnetite in the polymer can be achieved [9]. The polymer chosen for encapsulation in the studies discussed here is polystyrene, because it is cheap, well-known and can easily be functionalized by copolymerization [10], which allows us to answer the main question of this paper, which is the control and dependence of the amount of cell uptake by modification of the surface properties [11]. As polystyrene is not biodegradable it can be used for long term studies in animal models. Toxicity of polystyrene nanoparticles has been studied and although some toxicity was seen with nanoparticles in macrophages [12, 13], it appears to be less toxic than poly(methyl methacrylate) particles [14], which are under investigation for applications in humans.

Functionalization with acrylic acid leads to negatively charged particles containing carboxylic groups on the surface, which also offers the opportunity for further functionalization with biomolecules like amino acids or antibodies for targeting the particles. The surface charge can be changed by coupling lysine, glutamine or asparagine to the carboxylic groups by the known 1-ethyl-3-[3-dimethylaminopropyl]carbodiimide hydrochloride (EDC) coupling. Antibodies can be bound in the same way to the surface to modify the particles in biomedically interesting ways.

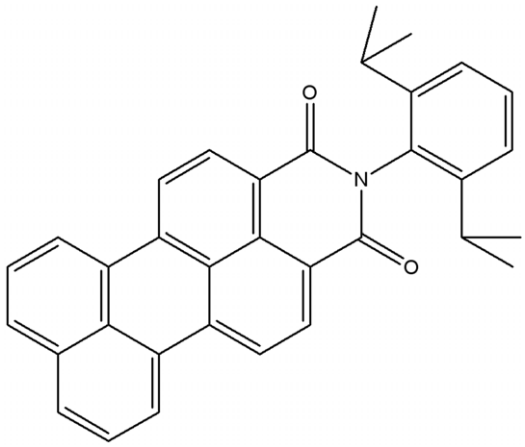


**Figure 1.** Chemical structure of the fluorescent dye PMI.

In this paper it is shown that it is possible to encapsulate high amounts of magnetite in carboxylated polystyrene and to control the number of carboxyl groups on the surface. To simplify the detection of the particles after uptake and detect the nanoparticles in two different ways, a hydrophobic fluorescent marker was also embedded in the polymer particles. These fluorescent and magnetic ('dual reporter') polystyrene particles were synthesized by a three-step miniemulsion route [9]. The surface charge was adjusted by varying the amount of carboxylated monomer used in the synthesis. Uptake into different cells was examined and the dependency of uptake on the surface charge was analysed. Lysine was also successfully covalently coupled to the particle surfaces and this efficiently changed the surface charge and cell uptake.

## 2. Experimental details

### *2.1. Materials*

Styrene and acrylic acid (Aldrich) were distilled under reduced pressure before use. All other chemicals were used as received: $FeCl_2 \cdot 4H_2O$ (Merck), $FeCl_3$ (Merck), ammonium hydroxide (Riedel-de-Haën, 26%), oleic acid (Merck), octane (Fluka, 96%), sodium lauryl sulfate (SDS) (Alfa Aesar, 99%), *N*-(2,6-diisopropylphenyl)-perylene-3,4-dicarbonacidimide (PMI) (BASF), 2,2′-azobis(2-methylbutyronitrile) (V59) (Wako Chemicals), hexadecane (HD) (Aldrich, 99%), 1-(3-dimethyl-aminopropyl)-3-ethylcarbodiimide hydrochloride (EDC) (Aldrich, 98%), *N*-hydroxysulfosuccinimide sodium salt (sulfo-NHS) (Fluka, 98.5%), (S)-(+)-lysine monohydrochloride (Merck). The surfactant Lutensol AT-50 (BASF) is a poly(ethyleneoxide)-hexadecyl ether with an EO block length of about 50 units. Demineralized water was used during the experiments. Poly-L-lysine (PLL, Sigma, Germany, MW 170 000) was used as transfection agent. In figure 1, the chemical structure of PMI is shown.

### *2.2. Synthesis*

The encapsulation of magnetite nanoparticles in a polystyrene shell was achieved by a three-step process [9]. The oleic acid coated magnetite nanoparticles were turned into a stable aqueous ferrofluid and then encapsulated via co-sonication with a styrene miniemulsion.

*2.2.1. Hydrophobic magnetite nanoparticles.* The magnetite nanoparticles were produced by coprecipitation of $Fe^{2+}/Fe^{3+}$. 14.6 g of $FeCl_3$ and 12.0 g $FeCl_2{\cdot}4H_2O$ were dissolved in 50 ml $H_2O$. 45 ml of ammonium hydroxide, 6 g of oleic acid was added, and the reaction mixture was heated up to 70 °C for 30 min under mechanical stirring. Then the temperature was increased to 110 °C in order to evaporate water and unreacted ammonia, and the black residue was dried overnight at 60 °C to give a black powder.

*2.2.2. Magnetite miniemulsion.* 1.0 g of the black magnetite powder was dispersed in 6.0 g octane. A solution of 721 mg of SDS in 24 g of $H_2O$ was added and the mixture mechanically stirred for 1 h for pre-emulsification. Then a miniemulsion was obtained by sonicating this emulsion twice for 2 min at 90% amplitude with a Branson sonifier (W450 digital, $1/2''$ tip) under ice-cooling in order to prevent uncontrolled polymerization.

In order to get a solvent-free system, octane was carefully evaporated by heating the system to 80 °C for 6 h. To compensate for the evaporation of water, approximately 2 ml of $H_2O$ were added every 30 min.

*2.2.3. Encapsulation of magnetite in polystyrene.* Styrene miniemulsions were prepared by mixing a hydrophobic phase containing styrene, 250 mg hexadecane, 100 mg initiator V59, 3 mg fluorescent dye PMI, and a solution of 72 mg of SDS in 24 g of $H_2O$. After pre-emulsification for 1 h, the miniemulsion was obtained by sonication under ice-cooling (2 min, 90%). For encapsulation, the miniemulsions of magnetite and styrene were mixed in a way that the ratio of magnetite powder to monomer was 1:1 and co-sonicated twice for 1 min at 50%. These miniemulsions were polymerized at 72 °C under mechanical stirring. After 6 h, the appropriate amounts of acrylic acid (0–15 wt% compared to styrene) were added and the polymerization was continued overnight.

An additional batch, VH3Ka, was synthesized with 3 wt% acrylic acid and no PMI for the use in cell-uptake experiments with lysine coupled to the surface or with poly-L-lysine (PLL) adsorbed to the particle surfaces.

*2.2.4. Functionalization of the nanoparticles.* 8.2 ml of the dialysed sample VH3Ka were ultracentrifuged for 40 min at 41 000 rpm. The precipitate was redispersed in 9 ml MES-buffer (10 mM, pH 6.5) to give a final solid content of 0.5%. 7.5 mg (39.4 $\mu$mol) EDC and 4.3 mg (19.7 $\mu$mol) sulfo-NHS were dissolved in 1 ml MES-buffer (10 mM, pH 6.5) and added to the dispersion. This mixture was stirred for 20 min, 7.2 mg (40 mmol) lysine was added, and the mixture was stirred for 3 h. Then the dispersion was again ultracentrifuged for 40 min at 41 000 rpm and the precipitate redispersed in demineralized water.

### *2.3. Characterization of particle properties*

The solid content of the final latexes was measured gravimetrically using a Kern RH 120-3 gravimeter. The average size and the $\zeta$-potential of the polymer particles were measured using a Zeta Nanosizer (Malvern Instruments, UK). An aqueous solution of KCl ($10^{-3}$ M) was applied for the $\zeta$-potential measurements.

The magnetite content was determined with an accuracy of about 1% by thermogravimetry of the dried samples. Thermogravimetric analyses were performed with a Mettler-Toledo TGA/SDTA851$^e$ under nitrogen atmosphere. The temperature range was from room temperature to 1100 °C at a heating rate of 10 °C $min^{-1}$. A distinction between maghemite and magnetite cannot be made by this method.

Preparative ultracentrifugation was used to get information about the distribution of magnetite particles in the polymer particles. Two drops of the sample were added to a tube containing a sucrose density gradient ranging from 1.0 to 1.3 g $cm^{-3}$ and centrifuged at 4 °C for 2 h at 37 000 rpm. After the centrifugation, the particles were collected in areas of the density gradient corresponding to their density. This means that pure polymer particles, composite particles and pure magnetite particles were separated after ultracentrifugation.

Information about the particle morphology was obtained by transmission electron microscopy (TEM) (Philips EM400). Each latex sample was diluted to about 0.01% solid content and a drop of it was placed on a carbon-coated copper grid. The sample was dried at ambient temperature and observed at an accelerating voltage of 80 kV. Additional contrasting was not applied.

After polymerization, SDS was removed by diafiltration (exclusion size of membrane 100 kDa) until the conductivity of water remained constant at a value $<3$ $\mu$S $cm^{-1}$. In the case of VHMPM0, VHMPM1 and VHMPM2, SDS was exchanged against a Lutensol AT-50-solution (0.05%, w/w).

The surface charge density was determined by streaming potential titration with a particle charge detector PCD 02 (Mütek GmbH, Germany). The measurements were performed with latex particles in aqueous solutions (about 1 g $l^{-1}$), using cationic polydiallyldimethyl ammonium chloride (PDADMAC) for titration.

Superconducting quantum interference device (SQUID) measurements were performed with a Quantum Design MPMS-5 SQUID magnetometer at 293 K.

### *2.4. Characterization of interaction of nanoparticles with cells*

*2.4.1. Cell culture.* HeLa cells were kept in Dulbecco's modified Eagle medium (DMEM) supplemented with 10% fetal calf serum (FCS), 100 units penicillin, 100 $\mu$g $ml^{-1}$ streptomycin, and 2 mM L-glutamine (all from Invitrogen, Germany). Mesenchymal stem cells (MSCs) were generated from bone marrow aspirations or explanted hips after obtaining informed consent. The study was approved by the ethics committee of the University of Ulm, Germany. Primary human MSCs were generated as previously described [15] and kept in $\alpha$-MEM (Cambrex, Belgium) supplemented with 20% FCS, 100 units penicillin, 100 $\mu$g $ml^{-1}$ medium streptomycin, and 1 mM pyruvate (Sigma, Germany). The MSCs showed an osteoblast, adipogenic and chondrogenic differentiation [15]. Jurkat cells were kept in Roswell Park Memorial Institute medium (RPMI, Invitrogen, Germany) supplemented with 10% FCS, 100 units penicillin, 100 $\mu$g $ml^{-1}$ medium streptomycin, and 2 mM L-glutamine and KG1a cells were kept in RPMI supplemented with 20% FCS, 100 units penicillin, 100 $\mu$g $ml^{-1}$ medium streptomycin, 2 mM L-glutamine, and 1 mM pyruvate.

The cells were grown in a humidified incubator at 37 °C and 5% $CO_2$. For the incubation, adherent cells were seeded at a density of 50 000 cells $cm^{-2}$ on the first day. Cells that were grown in suspension were seeded at a density of 1000 000 per ml. On the second day, the nanoparticles were added at a standard concentration of 75 $\mu$g Fe $ml^{-1}$ (also termed 1$x$ in the figures) to the media. Poly-L-lysine (PLL) was always added at a final concentration of 1.5 $\mu$g $ml^{-1}$ to the media. Adherent cells were trypsinized. The cells were then washed with phosphate buffered saline (PBS, Gibco, Germany), centrifuged and the pellet was resuspended in PBS for further analysis.

*2.4.2. FACS.* Fluorescent activated cell sorter (FACS) measurements were performed on a FACScan (Becton Dickinson, Heidelberg, Germany). Jurkat cells, KG1a cells, HeLa cells and MSCs were gated by sideward scatter versus forward scatter (SSC/FSC) plots. Fluorescence measurements were done in the FL1 channel.

In previous studies [10, 11] we had determined the amount of the fluorescent dye per weight of the nanoparticle preparation by absorption measurements as there was some coagulation during the polymerization process. In the particles used in the current experiments the iron oxide gave a broad peak in the absorption spectra, so the amount of the dye could not be determined. As there was no coagulation during the polymerization process it was assumed that there were equal amounts of the fluorescent dye per weight of polymer in this series of particles. Therefore the mean of the FL1 channel was normalized by the following formula in order to compare for efficiency of uptake of different particles:

$$\text{Normalized FL1} = n\text{FL1}_{(\text{particle } X)} = \frac{\text{MeanFL1}_{(\text{particle X})}}{\text{MeanFL1}_{(\text{uncharged particle})}}.$$

*2.4.3. Confocal laser scanning microscopy.* Intracellular localization was confirmed by confocal laser scanning microscopy (LSM Fluoview on a IX71 with two lasers (488 nm and 543 nm) and a 60× oil lens, (Olympus Hamburg, Germany)). Fluorescent labelled nanoparticles were excited with 488 nm and detected in channel 1 (mirror 570 nm, filter 530 nm). During a second scan the red fluorescent dye RH414 (Molecular Probes, Eugene, OR) as marker for cell membranes was excited by the 543 nm laser and detected in channel 2 (filter 565 nm). Three acquisitions were averaged according to the Kalman algorithm.

*2.4.4. Transmission electron microscopy.* The cells were fixed with 2.5% glutaraldehyde (Fluka, Germany), containing 1.5% saccharose in PBS (pH 7.3), and postfixed in 2% aqueous osmium tetroxide (Fluka, Germany). The samples were then dehydrated in graded series of 1-propanol and block stained in 1% of uranyl acetate and embedded in Epon (Fluka, Germany). Ultrathin sections (80 nm) were contrasted with 0.3% lead citrate and imaged in a Philips 400 TEM (Fei, Eindhoven, The Netherlands) at an accelerating voltage of 80 kV.

*2.4.5. Prussian blue staining.* For Prussian blue staining, the cells were fixed in methanol for 10 min, incubated in freshly prepared potassiumhexacyanoferrate(II) solution (Sigma, Taufkirchen, Germany, 2% w/w, with 0.1 N HCl) for 10 min and counterstained with hematoxylin–eosin (Fluka, Germany).

*2.4.6. Quantitative iron measurement by a ferrozine assay.* For quantitative measurements an aliquot of the cells was counted with TrueCount beads (BD, Germany) in triplicate. The pellets were dried at 96 °C overnight and digested in a mixture (50 $\mu$l) of perchloric and nitric acid at a ratio of 3:1 at 56 °C for at least 3 h. Aliquots were diluted 1:20 and were used in a ferrozine based quantitative iron kit (Nobiflow Iron, Hitado Diagnostics Möhnesee, Germany). Magnetite containing particles of known iron content were digested and diluted to obtain a standard curve.

## 3. Results and discussion

A series of fluorescent composite 'dual reporter' latex particles consisting of magnetite and poly(styrene-*co*-acrylic acid) was synthesized in a three-step miniemulsion process to obtain particles with high amounts and homogeneous distribution of encapsulated magnetite. Additionally, a fluorescent dye was incorporated to simplify detection of the particles after cell uptake by FACS measurements and laser scanning microscopy (LSM). The amount of fluorescent dye was kept constant at about 3 mg per reaction mixture. In order to prevent polymerization of the hydrophilic monomer acrylic acid in the water phase and in order not to charge the particles negatively by initiator molecules on the surface, the oil-soluble initiator

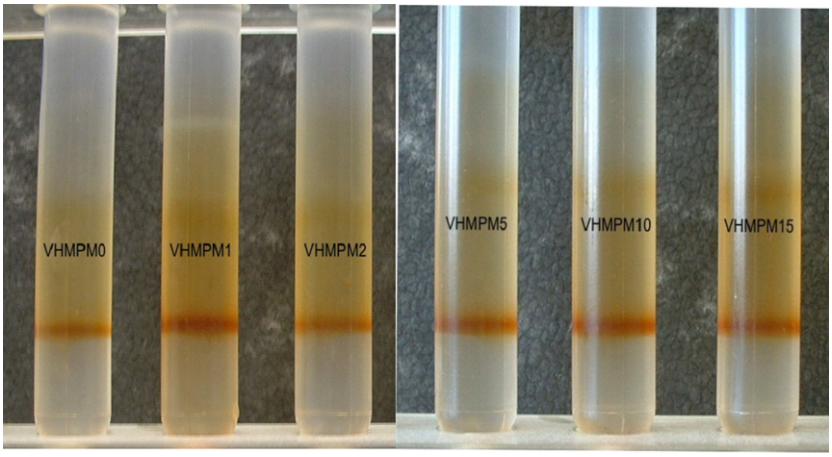


**Figure 2.** Encapsulation of magnetite as shown by ultracentrifugation experiments in a density gradient for the samples with different acrylic acid contents (0–15%).

**Table 1.** Characteristics of the magnetic and fluorescent latexes.

| Sample | Acrylic acid content (%) | Solid content (%) | Diameter[a] (nm) | Polydispersity index (PDI) | Solid content after dialysis (%) | Magnetite content[b] (%) | Surface charge[c] ($nm^{-2}$) |
|---|---|---|---|---|---|---|---|
| VHMPM0 | 0 | 6.82 | 57 | 0.254 | 1.20 | 30 | 0.100 |
| VHMPM1 | 1 | 7.51 | 53 | 0.336 | 1.02 | 40 | 0.107 |
| VHMPM2 | 2 | 6.91 | 45 | 0.219 | 1.23 | 36 | 0.117 |
| VHMPM5 | 5 | 7.57 | 52 | 0.198 | 0.18 | 35 | 0.378 |
| VHMPM10 | 10 | 7.31 | 46 | 0.195 | 0.08 | 36 | 0.803 |
| VHMPM15 | 15 | 6.81 | 67 | 0.197 | 0.19 | 39 | 1.463 |
| VH-3Ka | 3 | 8.91 | 68 | 0.374 | 0.18 | 28 | 0.537 |

[a] Determined by DLS.
[b] Determined by TGA.
[c] Determined by surface charge titration.

V59 was used. As stabilizer both for magnetite miniemulsion and the composite miniemulsion, the anionic surfactant SDS was used, which had to be washed off using a size exclusion membrane before further characterization. In table 1, the solid content before and after washing, the particle size, the polydispersity index (PDI), the magnetite content and the surface charge of the hybrid nanoparticles are shown.

The size of the particles was measured by dynamic light scattering. Regardless of the concentration of the functional monomer, the particle diameter ranged from 45 to 70 nm. The particle size in relation to the concentration of acrylic acid added to the reaction mixture did not change significantly with increasing amount of acrylic acid.

The magnetite content of the final particles as determined by TGA measurements under nitrogen atmosphere was between 30% and 40%.

It was shown by preparative ultracentrifugation in a density gradient that the encapsulation was homogeneous and pure polymer particles were not detected. All of the latexes showed a narrow density distribution (see figure 2), which indicated that all final nanoparticles contained nearly the same polymer to magnetite ratio.

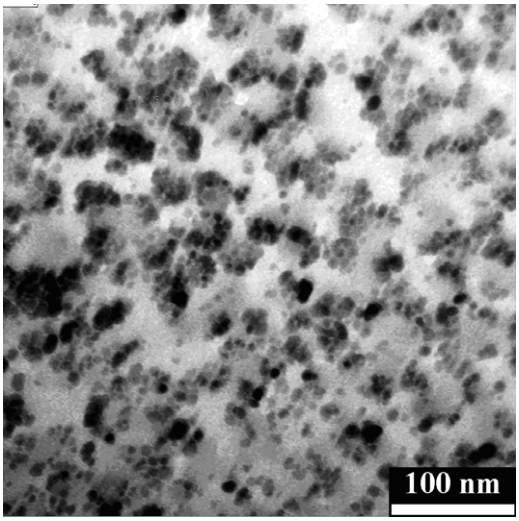


**Figure 3.** TEM pictures of encapsulated magnetite particles with 1% of acrylic acid (VHMPM1).

It can also be seen that, as expected, the density of the composite particles did not change with the amount of acrylic acid. As acrylic acid was added to the reaction mixture 6 h after the polymerization had started, this component was not supposed to affect the encapsulation process significantly and only to functionalize the particle surfaces.

In figure 3, a TEM picture of a sample with 1% acrylic acid (VHMPM1) is shown. The arrangement of magnetite particles in polystyrene shells can be seen. As expected, the diameter of the visible (hard) spheres is smaller than the (hydrodynamic) diameter obtained in DLS measurements.

The surface charge is a property that is very interesting for cell uptake. We have shown earlier that the amount of surface charge influences the cell uptake [10]. Cell uptake increases with increasing surface charge up to a certain charge concentration.

The surface charge density of the magnetite containing hybrid particles was determined by particle charge detection. The results are shown in figure 4. Generally, the surface charge of the particles decreases with increasing amount of acrylic acid added during the reaction. The surface charge of pure poly(styrene-*co*-acrylic acid) particles (without magnetite) has been determined earlier [10], and it was found that the numbers of surface charges of the composite particles containing the magnetite are lower than those of the polymer particles although the same ratio of polystyrene/acrylic acid was used.

As hydrophilic magnetite particles are encapsulated in the composite particles, there are two interfaces between polymer and hydrophilic material, i.e. magnetite particles or the water phase. Therefore the carboxylic groups do not only tend to be arranged on the polymer/water interface, but also inside the particle on the polymer/magnetite interface. This explains why about 30% fewer carboxylic groups are found on the surface of the particles compared to poly(styrene-*co*-acrylic acid) particles without magnetite (data also shown in figure 4) [10].

The magnetic properties of the latexes are highly interesting for further applications. In table 2, the results of the magnetic measurements on the initial magnetite nanoparticles and some of the magnetic polystyrene particles are summarized. All latexes show typical superparamagnetic behaviour at room temperature without a hysteresis loop. This indicates that the magnetic particles are still separated in the polymer matrix of the composite particles.

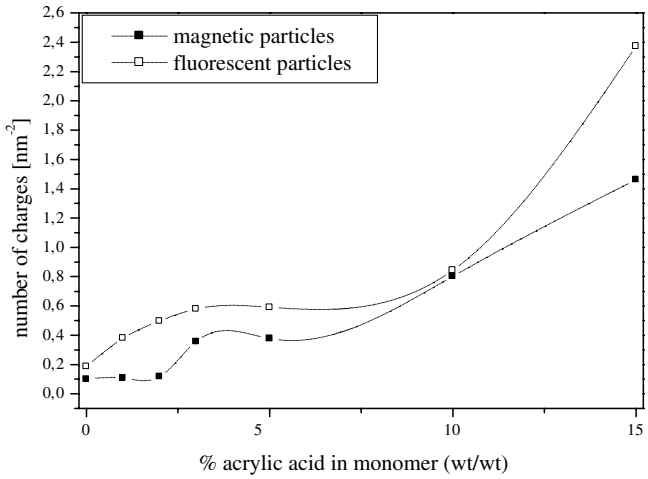


**Figure 4.** Surface charge density versus concentration of acrylic acid for the magnetic particles (the lines are guides to the eye). The comparison with the fluorescent particles without encapsulated magnetite [10] shows that in the case of the magnetite containing latexes the carboxylic group on the surface is reduced by about 30%.

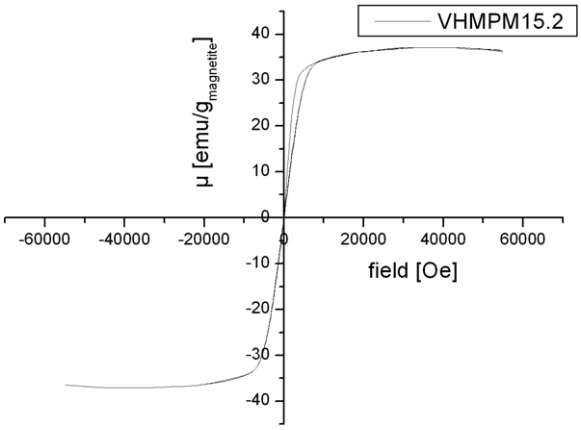


**Figure 5.** Magnetic field dependence of encapsulated magnetite particles with 15% of acylic acid.

**Table 2.** Magnetic properties of the particles.

| Sample | Saturation magnetization $M_S$ (emu g$^{-1}$ magnetite) | Initial susceptibility (emu Oe$^{-1}$) |
|---|---|---|
| Magnetite particles | 80.43 | 0.029 |
| VHMPM0 | 35.56 | 0.013 |
| VHMPM1 | 44.70 | 0.017 |
| VHMPM5 | 37.26 | 0.013 |
| VHMPM15 | 37.07 | 0.013 |

In figure 5, the magnetization curve of the latex with 15% of acrylic acid (VHMPM15) is shown as representative for all latexes.

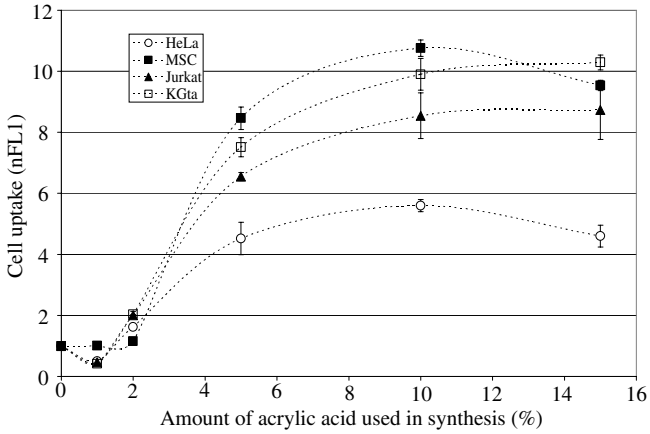


**Figure 6.** Uptake of VHMPM particles in different cell lines. Different cell lines show similar results for the uptake of VHMPM particles by FACS. HeLa (open circle, ○), MSC (filled square, ■), KG1a (open square, □), Jurkat (filled triangle, ▲). Lines are given as guides for the eye.

The saturation magnetization of the oleic acid coated magnetite particles is close to the saturation magnetization of bulk material (89 emu $g^{-1}$) [9] and higher than that of the encapsulated magnetite particles with different amounts of acrylic acid (VHMPM0 to VHMPM15). This indicates that during preparation of the magnetite miniemulsion some of the magnetite is oxidized to nonmagnetic iron oxide phase. No more magnetization is lost during polymerization, so no further oxidation seems to happen.

Sample VH3Ka was used to covalently bind lysine on the surface of the nanoparticles (VH3KaLys). Here, lysine was bound by the EDC coupling, using sulfo-NHS as catalyst. $\zeta$-potential measurements of the latexes before and after coupling of lysine show that the coupling was successful: the $\zeta$-potential after the coupling was more positive (before coupling: $-47.5$ mV; after coupling: $-10.9$ mV). In addition, the hydrodynamic diameter of the particles was more than doubled (before coupling: 68 nm; after coupling: 151 nm).

In order to evaluate these nanoparticles as dual-use reporters (fluorescence measurements for histological assessments and the superparamagnetic component for MRI detection), these nanoparticles were incubated with different cell types. Incubation was for 24 h in protein containing medium (fetal calf serum; for details see section 2). As readout, a fluorescent activated cell sorter (FACS) was used to compare the uptake of the differently functionalized nanoparticles (see figure 6). In order to compare the uptake of the nanoparticles, the fluorescent intensity was normalized by the equation given in section 2.4.2. As can be seen in figure 6, there is an increase of uptake of nanoparticles from uncharged particles (VHMPM0) to the higher charged particles which is consistent for MSC, HeLa, Jurkat and KG1a cells.

The intracellular uptake of the 'dual reporter' particles was demonstrated by laser scanning microscopy (LSM). It has to be noted that all these experiments were done without the addition of a transfection agent, thereby relying completely on the properties of the nanoparticle surface as it has been synthesized in the miniemulsion process, i.e. the carboxylated surface modification. The outer cell membrane was stained with a fluorescent dye (RH414, shown in red, figure 7). All particles are clearly located within these boundaries (green). There are no yellow pixels in the overlay which would indicate colocalization of cell membrane (red channel) and nanoparticle (green channel) in these pixels.

It was tried to measure the iron content in these cell cultures; however, it was not possible to find a detectable amount of iron (not shown). So, the positively charged PLL was used as a

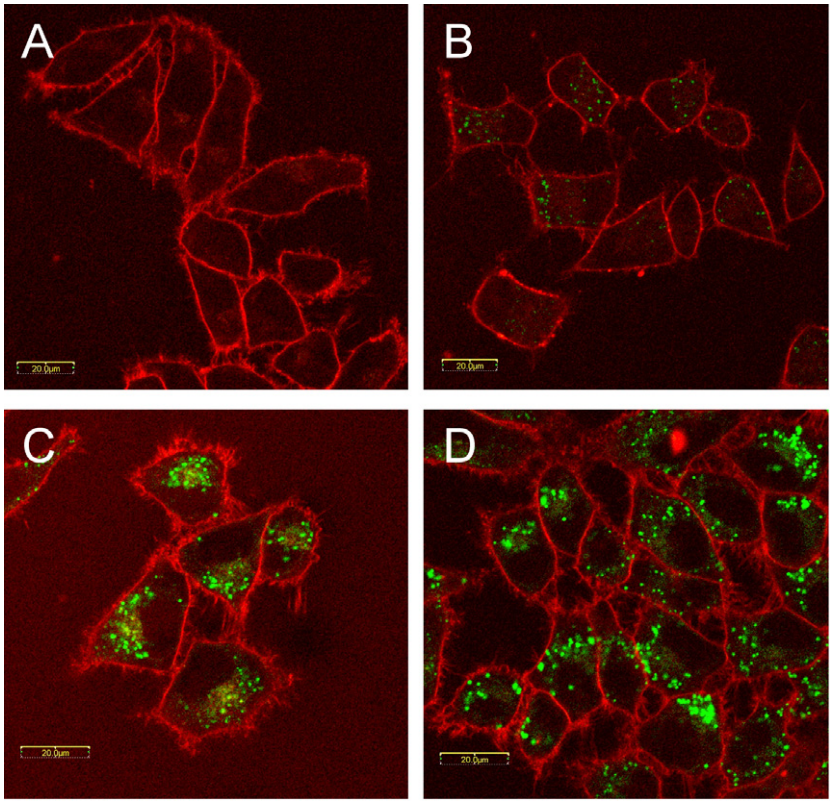


**Figure 7.** Laser scanning microscopy of HeLa cells. Cell membranes are stained with RH414 in red (contours) and the particles in green (dots in the cells). (A) Untreated control, (B) VHMPM2 (2% of acrylic acid), (C) VHMPM5 (5% of acrylic acid), (D) VHMPM10 (10% of acrylic acid).

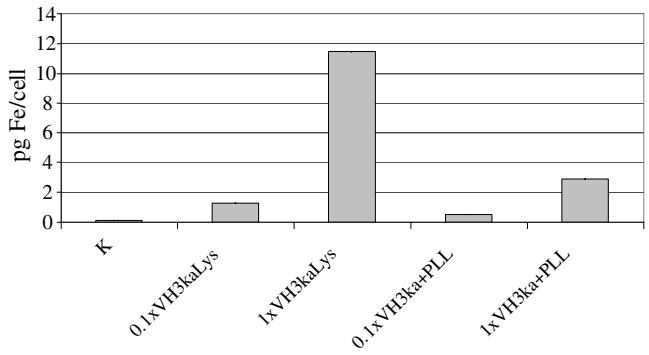


**Figure 8.** Iron uptake of lysine functionalized particles (VH3kaLys) and carboxyl functionalized particles with poly-L-lysine as transfection agent (VH3ka + PLL). Uptake depends on concentration of nanoparticles ($0.1x$ equals 7.5 $\mu$g nanoparticles ml$^{-1}$, $1x$ equals 75 $\mu$g nanoparticles ml$^{-1}$).

transfection agent to enhance the intracellular uptake of these nanoparticles [16] as positively charged side groups enhance cellular uptake even more efficiently [11]. Not surprisingly, as demonstrated in figure 8, the uptake of iron depends on the concentration of the hybrid

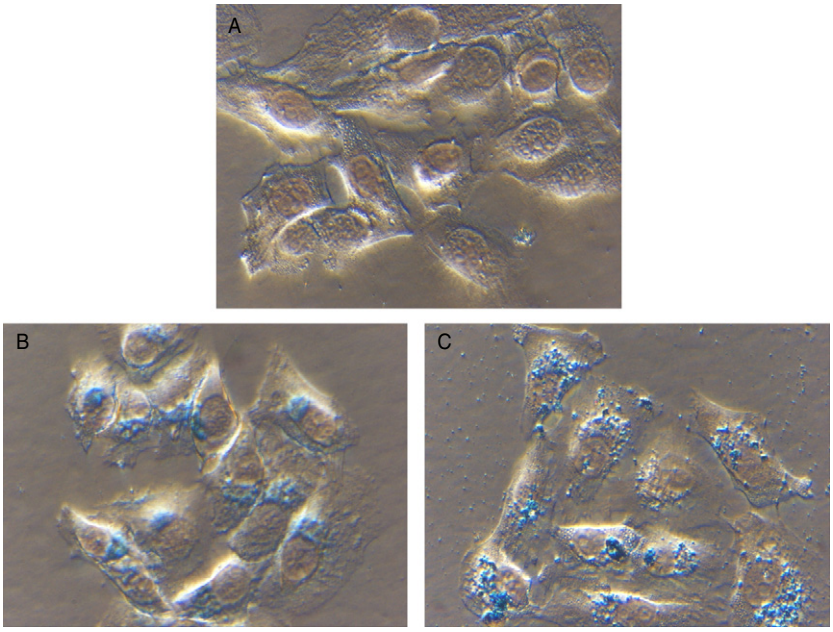


**Figure 9.** Prussian blue staining of VH3ka and VH3kaLys in HeLa. While there are no blue spots in A (control cells), there are bluish spots in VH3ka when PLL (B) was added and VH3kaLys (C) even without the addition of a transfection agent.

nanoparticles in the cell culture medium ($0.1x$ equals 7.5 $\mu$g nanoparticles ml$^{-1}$, $1x$ equals 75 $\mu$g nanoparticles ml$^{-1}$). The transfection functionality can also be grafted (and therefore covalently bonded) onto the surface of the nanoparticles as lysine functionalized nanoparticles show the same dependence of concentration with an even higher amount of measurable iron content in these cell cultures (up to 11 pg/cell, figure 8). This means that the particles with coupled lysine are best suited for cell uptake.

Detection of these particles was also done by means of light microscopy. The cells were stained for iron by a Prussian blue reaction and counterstaining was done by a standard hematoxylin–eosin staining. Figure 9 demonstrates the uptake of iron oxide particles in HeLa cells. Only in cell cultures with iron oxide containing nanoparticles with a transfection agent (figure 9(B)) or with the lysine functionalized nanoparticles (figure 9(C)) was there a detectable amount of iron as demonstrated by the bluish precipitates.

Subcellular detection for these nanoparticles was also investigated by transmission electron microscopy. The lysine functionalized nanoparticles (VH3kaLys) were detected as electron dense conglomerates (dark spots) in endosomal compartments of MSC (figure 10(A), arrows). Figure 10(B) demonstrates that these nanoparticles are engulfed by the cell membrane. This can be interpreted as an endocytotic process. In the case of the carboxylated particles (VH3ka) with PLL, intracellular and extracellular nanoparticles were found (figures 10(C) and (D)). Lead citrate counterstaining in figures 10(C) and (D) results in better delineation of cellular and intracellular membranes and higher electron densities of the content of some intracellular compartments (figures 10(C) and (D) white arrowheads), but still the iron containing VH3ka (black arrows) can be distinguished by the difference in appearance. In none of these electron dense bodies were nanoparticles detected. Also note that the particles are aggregated in figure 10(D).

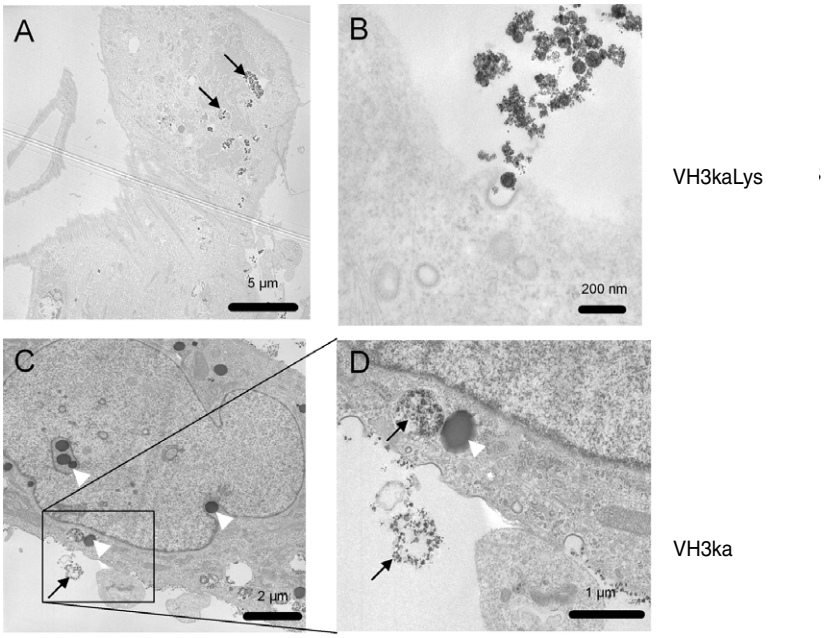


**Figure 10.** TEM studies of VH3ka (A) and (B) and VH3kaLys (C) and (D) in MSC. (A) and (B) were not counterstained with lead citrate. The dark spots in A (arrows) correspond to VH3kaLys in endosomes. (C) and (D) are counterstained with lead citrate and therefore cell organelles appear darker (white arrowheads), but still the iron containing VH3ka (black arrows) can be distinguished. (D) is a magnification of (C).

## 4. Conclusion

A series of polystyrene particles containing two reporters–magnetite nanoparticles and a fluorescent dye–was synthesized in a three-step miniemulsion process. Designing of the surface with defined amounts of carboxylic acid groups was achieved by copolymerization with acrylic acid. It was shown that the number of surface charges depends on the amount of acrylic acid used. The magnetization measurements demonstrated that the paramagnetic behavior is maintained during polymerization, which means that the magnetite nanoparticles are well separated within the polymeric shell. Uptake of these nanoparticles is dependent on the amount of carboxylic groups on the surface. An increase of carboxylic surface groups leads also to a significant increase in the uptake behaviour in endosomal compartments, as demonstrated by LSM and TEM. Further modification of the surface was achieved by physically adsorbing poly-L-lysine or covalently coupling lysine to the surface. The positively charged transfection functionalities leads to an increased uptake: the best uptake for the nanoparticles was obtained by the covalent lysine modification, in which high amounts of iron can be detected in the cells, which makes them suitable for a wide range of biomedical applications such as use as a contrast agent for magnetic resonance imaging, hyperthermia and selection of cells.

## References

[1] Pankhurst Q A, Connolly J, Jones S K and Dobson J 2003 Applications of magnetic nanoparticles in biomedicine *J. Phys. D: Appl. Phys.* **36** R167–81

[2] Schroeder U, Sommerfeld P, Ulrich S and Sabel B A 2000 Nanoparticle technology for delivery of drugs across the blood-brain-barrier *J. Pharm. Sci.* **87** 1305–7

[3] Sundstrom J B *et al* 2004 Magnetic resonance imaging of activated proliferating rhesus macaque T cells labeled with superparamagnetic monocrystalline iron oxide nanoparticles *J. Acquir. Immune Defic. Syndr.* **35** 9–21
[4] Hilger I, Hergt R and Kaiser W A 2005 Use of magnetic nanoparticle heating in the treatment of breast cancer *IEE Proc. Nanobiotechnol.* **152** 33–9
[5] Berry C C and Curtis A S G 2003 Functionalisation of magnetic nanoparticles for applications in biomedicine *J. Phys. D: Appl. Phys.* **36** R198–206
[6] Alexiou C *et al* 2000 Locoregional cancer treatment with magnetic drug targeting *Cancer Res.* **60** 6641–8
[7] Hilger I *et al* 2001 Electromagnetic heating of breast tumors in interventional radiology: in vitro and in vivo studies in human cadavers and mice *Radiology* **218** 570–5
[8] Landfester K and Ramírez L P 2003 Encapsulated magnetite particles for biomedical application *J. Phys.: Condens. Matter* **15** 1345–61
[9] Ramírez L P and Landfester K 2003 Magnetic polystyrene nanoparticles with a high magnetite content obtained by miniemulsion processes *Macromol. Chem. Phys.* **204** 22–31
[10] Holzapfel V, Musyanovych A, Landfester K, Lorenz M R and Mailänder V 2005 Preparation of fluorescent carboxyl and amino functionalized polystyrene particles by miniemulsion polymerization as markers for cells *Macromol. Chem. Phys.* **206** 2440–9
[11] Lorenz M R *et al* 2006 Uptake of functionalized, fluorescent-labeled polymeric particles in different cell lines and stem cells *Biomaterials* **27** 2820–8
[12] Hamoir J *et al* 2003 Effect of polystyrene particles on lung microvascular permeability in isolated perfused rabbit lungs: role of size and surface properties *Toxicol. Appl. Pharmacol.* **190** 278–85
[13] Olivier V *et al* 2003 Comparative particle-induced cytotoxicity towards macrophages and fibroblasts *Cell. Biol. Toxicol.* **19** 145–59
[14] Horowitz S M, Gautsch T L, Frondoza C G and Riley L Jr 1991 Macrophage exposure to polymethyl methacrylate leads to mediator release and injury *J. Orthop. Res.* **9** 406–13
[15] Pittenger M F and Martin B J 2004 Mesenchymal stem cells and their potential as cardiac therapeutics *Circ. Res.* **95** 9–20
[16] Arbab A S *et al* 2003 Characterization of biophysical and metabolic properties of cells labeled with superparamagnetic iron oxide nanoparticles and transfection agent for cellular MR imaging *Radiology* **229** 838–46